

# What the Optical Recombination Lines Can Tell Us About the Broad-Line Regions of Active Galactic Nuclei

Kirk T. Korista

*Department of Physics, Western Michigan University  
Kalamazoo, MI 49008-5252*

korista@wmich.edu

and

Michael R. Goad

*Department of Physics and Astronomy, University of Southampton  
Highfield, Southampton, SO17 1BJ, England, UK*

mrg@astro.soton.ac.uk

## ABSTRACT

We investigate the effect of a global change in the ionizing continuum level on the behavior of the strong optical broad emission lines seen in spectra of the nuclear emission-line regions of active galactic nuclei (AGN), including the Balmer lines, He I  $\lambda 5876$ , and He II  $\lambda 4686$ . Unlike most of the prominent heavy element lines found in the UV, the optical hydrogen and helium recombination lines' emissivities are strongly dependent on the incident continuum flux, since these lines arise out of excited states whose *optical depths depend on the incident flux of photons*. Using photoionization calculations we determine the luminosity-dependent responsivities,  $\eta(r, L(t)) = \Delta \log L_{line} / \Delta \log L_{cont}$ , of these lines for a general model of the broad emission line region (BLR), with the purpose of establishing them as important probes of the physical conditions within the BLR of AGNs. The dependence of these lines' emissivities on the incident photon flux invokes a dependence in their responsivities on distance from the central continuum source. In particular, the responsivities of these lines are generally anticorrelated with the incident photon flux. Thus, their responsivities vary with distance within the BLR for a fixed continuum luminosity and change with time as the continuum source varies. Consequently, after correcting for light-travel-time effects the response of the Balmer and optical helium lines should generally be strongest during low continuum luminosity states. Responsivity that depends on photon flux and continuum state may explain a number of outstanding problems currently under investigation in broad-line variability studies of these and other emission lines. These include the origin of the intrinsic Baldwin effect, measurements of luminosity-dependent lags (a "breathing" BLR) and luminosity-dependent variations in: integrated broad emission-line flux ratios (including He II  $\lambda 4686/H\beta$ ), broad line profile shapes, and radial velocity-dependent intensity ratios. The broad  $H\alpha/H\beta$  and He I/ $H\beta$  flux ratios and the Balmer emission-line responsivity are observed to decrease from the line center to the line wings. These, along with our findings, lead to the conclusion that the BLR velocity field diminishes with increasing distance from the central continuum source. This is consistent with recent reverberation studies that find a relationship between the emission-line lag and rms profile width for multiple lines in individual AGN, which implies that the velocity field is dominated by a central massive object. Finally, the responsivity of ionization-bounded clouds can account for much of the observed behavior of the optical recombination lines (e.g., the weak response of the Balmer line wings) previously attributed to a substantial contribution from matter-bounded clouds at small BLR radii.

*Subject headings:* galaxies: active—galaxies: nuclei<sup>1</sup>—galaxies: Seyfert— (galaxies:) quasars: emission lines—line: formation—line: profiles

## 1. INTRODUCTION

Historically, attempts at interpreting the observed variability behavior of the broad emission lines in active galactic nuclei (AGN) have tended to regard the broad emission line region (BLR) as a stationary entity (non-evolving). By this we mean that any variability in the observed emission-line intensities has been attributed solely to reverberation (light-travel-time) effects within a spatially extended BLR. Thus, variations in the measured BLR sizes and the amplitude of the line response have been assumed to arise primarily through differences in the temporal variability of the ionizing continuum, which manifests as a difference in shape and FWHM of the continuum autocorrelation function (ACF) from one event to the next (e.g., Pérez, Robinson, & de la Fuente 1992). In essence, higher frequency continuum variations are better able to probe smaller BLR sizes, while larger BLR sizes are better probed by lower frequency continuum variations.

While a difference in the continuum variability time scale (e.g., the width of the continuum ACF) explains in part some of the observed variability seen in the broad emission lines in AGNs, it is by no means the complete picture. Indeed, more sophisticated photoionization calculations (e.g., see Krolik et al. 1991; O’Brien et al. 1995; Bottorff et al. 1997; Kaspi & Netzer 1999; Horne, Korista, & Goad 2003) have modeled the line variability by including the local emission-line response to changes in the overall luminosity and/or shape of the ionizing continuum. The models presented by Carroll (1985) and Netzer (1991) anticipated the non-linear response of some of the emission lines.

In this paper we illustrate, using a general description of the BLR, how large changes in the mean continuum level may explain much of the observed variability behavior of the optical recombination lines. In § 2 we describe the grid of photoionization models used in this study. In § 3 we describe the physical origin of line responsivity and its impact on the following issues related to BLR variability: the origin and slope of the intrinsic Baldwin effect (§ 3.2; e.g., Kinney, Rivolo, & Koratkar 1990); variations in the measured continuum–emission-line time-delays (§ 3.3; e.g., Peterson et al. 2002), variations in the emission line flux ratios (§ 3.4; e.g., Balmer decrement:

Tran, Osterbrock, & Martel 1992;  $H\beta/He\ II\ 4686$ : Peterson & Ferland 1986); changes in profile shape (§ 3.5; e.g., Wanders & Peterson 1996); and velocity-dependent line intensity ratios (§ 3.6; e.g., Stirpe, de Bruyn, & van Groningen 1988). We emphasize that the variations in these quantities discussed here are *not* a consequence of reverberation effects within a finite-sized BLR, although they are intimately related. Rather, they are due to global changes in the mean ionization state of the BLR gas. In § 4 we discuss the impact of these findings on the purported contribution of a very broad optically thin component to the emission-line response, and other related issues. It is our hope that many of these observed emission-line variations and trends reported in the literature may be examined in a new light. We summarize our main findings in § 5.

## 2. PHOTOIONIZATION MODELS

### 2.1. The Grid of Photoionization Models

For the purposes of demonstration, we adopted the grid of photoionization computations presented in Korista & Goad (2000; hereafter KG00) that they used to model the strong UV broad emission lines of NGC 5548. The reader is directed there for details; here we mention some of the salient features of their grid and adopted model.

Using Ferland’s spectral synthesis code, Cloudy (v90.04; Ferland 1997; Ferland et al. 1998), KG00 generated a grid of 3249 photoionization models of broad line-emitting entities, here assumed to be simple, single total hydrogen column density slabs ( $N_H = 10^{23}\text{ cm}^{-2}$ ), each of which has constant gas density (for simplicity) and a clear view to the source of ionizing photons. The grid dimensions spanned 7 orders of magnitude in total hydrogen gas number density,  $7 \leq \log n_H(\text{cm}^{-3}) \leq 14$ , and hydrogen-ionizing photon flux,  $17 \leq \log \Phi_H(\text{cm}^{-2}\text{ s}^{-1}) \leq 24$ , and stepped in 0.125 decade intervals in each dimension. We refer to the plane defined by these two parameters as the density-flux plane. The choice of spectral energy distribution (SED) is described in KG00 (see also Figure A1 in Horne, Korista, & Goad 2003). In the Appendix we discuss the sensitivity of the results presented here to these and other assumptions.

In the top four panels of Figure 1 we show the equivalent width (EW) distributions of the prominent optical broad emission lines of H $\alpha$   $\lambda$ 6563, H $\beta$   $\lambda$ 4861, He I  $\lambda$ 5876, and He II  $\lambda$ 4686, namely, those of primary interest in the present paper. These EWs are all referenced to the same incident continuum flux at 1215 Å and *are a measure of the efficiency by which ionizing continuum photons are converted into line photons*. The peak in the EW distribution for each line is denoted by a triangle. Note that the EWs of the Balmer and He I lines increase with increasing density, especially at the lower values of the photon flux, illustrating the effects of collisional excitation from excited states (Ferland & Netzer 1979). In every case, the line EWs decline in the direction of increasing ionizing photon flux for values greater than those marking the peak EWs:  $\log \Phi_H = 17.125, 18.250, 19.125,$  and  $20.750$  for H $\alpha$ , H $\beta$ , He I, and He II, respectively. The rapid decline in the line EWs of the two Balmer lines for  $\log \Phi_H \approx \log n_H + 10.25$  is due to the hydrogen in the fixed-column density slabs becoming fully ionized, a subject we discuss later. The two helium lines do likewise at slightly larger values of  $\log(U_{HC}) \equiv \log \Phi_H - \log n_H$ . The upper left corners of these diagrams represent gas near the Compton temperature. Detailed discussions of these and other EW contour plots in the density-flux plane can be found in Korista et al. (1997). In order to aid in comparison and to serve as a fixed point of reference, the star symbol in each of the panels shows the location of the standard BLR parameters from Davidson & Netzer (1979).

The EW distributions of two other hydrogen recombination lines, H $\gamma$   $\lambda$ 4340 and Ly $\alpha$   $\lambda$ 1216<sup>1</sup>, are plotted in the bottom panels of Figure 1. We refer to them from time to time for purposes of comparison.

## 2.2. A Simple Model for the BLR of NGC 5548: A Test Case

To model the mean UV spectrum of NGC 5548 from the 1993 *HST* campaign (Korista et al. 1995; hereafter K95) KG00 took the “locally optimally-emitting clouds” (LOC) approach of Baldwin et al. (1995) by summing the emission from a weighted distribution of “clouds” along the two dimensions

<sup>1</sup>This is a sum of Ly $\alpha$  and minor contributions from O V]  $\lambda$ 1218 and He II  $\lambda$ 1216.

of gas density and radius; KG00 assumed constant column density clouds of  $10^{23} \text{ cm}^{-2}$ . The cloud distribution functions in gas density and radius are described in KG00. In brief, the model-integrated spectra included clouds spherically distributed around the continuum source whose gas densities<sup>2</sup> and distances from the central source of ionizing photons spanned  $8 \leq \log n_H \text{ (cm}^{-3}\text{)} \leq 12$  and 1–140 lt-days; very highly ionized clouds ( $\log U_{HC} > 11.25$ ) were excluded from the integration (see KG00 for details). Asymmetric geometric effects, such as emission-line anisotropy (Ferland et al. 1992; O’Brien et al. 1994), were not considered. KG00 showed that this simple model with widely distributed cloud properties was also generally successful in reproducing the observed UV broad emission-line variability.

With the choice of cosmological parameters and adopted Galactic reddening along the line of sight to NGC 5548 from KG00, the mean value of  $\lambda F_\lambda(1350)$  continuum flux from the 1993 *HST* campaign (K95) corresponds to  $\log \lambda L_{\lambda 1350}(\text{ergs s}^{-1}) \approx 43.54$ . Using the central continuum SED adopted by KG00, the corresponding mean hydrogen-ionizing luminosity from the 1993 *HST* campaign is  $\log L_{ion}(\text{ergs s}^{-1}) \approx 44.26$ . At this luminosity a hydrogen-ionizing photon flux  $\log \Phi_H(\text{cm}^{-2} \text{ s}^{-1}) = 20$  corresponds to a distance from the continuum source of  $R \approx 12.6(75/H_o)$  lt-days, and the model BLR spans  $\log \Phi_H(\text{cm}^{-2} \text{ s}^{-1}) \approx 17.9$  to  $\approx 22.2$  in this mean continuum state. In this paper we consider two historical extrema in the  $\lambda F_\lambda(1350)$  continuum flux of NGC 5548 about the above mean level. In 1992, the continuum went into a very low state,  $\log \lambda L_{\lambda 1350}(\text{ergs s}^{-1}) \approx 42.90$ , while a high state of  $\log \lambda L_{\lambda 1350}(\text{ergs s}^{-1}) \approx 43.81$  was recorded during the 1989 campaign. This is a factor of about 8.2 change in the continuum flux at 1350 Å, and we assumed that the SED did not change shape.

While we do present results based on a simple LOC model of the BLR in NGC 5548, they should be representative of most general classes of models describing the broad emission lines. The major trends should be largely model-independent, while the details should be diagnostic of the physical

<sup>2</sup>Given the choice of a single cloud column density and the assumption of constant hydrogen gas densities within the cloud, the cloud radial thicknesses range over  $10^{11} - 10^{15} \text{ cm}$ .

conditions within individual BLRs.

### 3. EMISSION-LINE RESPONSIVITY

Summing the line emission along the cloud gas density distribution at each radius, we can derive an effective cloud surface flux of the emission lines at that radius (see KG00; Baldwin et al. 1995). Figure 2 shows the surface flux of  $H\beta$  as a function of radius from the central continuum source for each of the two continuum states. The slope of cloud emission-line surface flux plotted against the ionizing flux ( $\propto L_{ion}/r^2$ ) is a measure of the effective radial responsivity of the emitting gas for small amplitude (or equivalently, short time scale) changes in the ionizing continuum (see Goad et al. 1993). Similarly, the difference in the two surface flux curves plotted in Figure 2 (in  $\log_{10}$  space) relative to the logarithm of the factor of 8.2 in the incident continuum flux measures a “global” response to long-term, large amplitude, changes in the continuum state. We define this responsivity parameter as

$$\eta(r) = \frac{\Delta \log F(r)_{line}}{\Delta \log \Phi_H}. \quad (1)$$

This definition of line responsivity converges to the definition given in Goad et al. (1993) for very small variations in the continuum flux<sup>3</sup>. Note that the upper curve in Figure 2 is essentially the lower curve shifted along the x-axis by  $0.5 \times \log(8.2)$  decades. A logarithmic slope of  $-2$  in Figure 2 corresponds to  $\eta(r) = 1$ , whereas flatter slopes correspond to  $\eta(r) < 1$ . When integrated over the full line-emitting region, what we call the effective responsivity,  $\eta_{eff}$ , is the logarithmic slope in the relation  $L_{line} \propto L_{cont}^{\eta_{eff}}$ .

The solid curves in Figure 3 illustrate the global responsivities as functions of radius of  $H\beta$  (*bottom left*),  $H\alpha$  (*top left*),  $He\ I\ \lambda 5876$  (*top right*), and  $He\ II\ \lambda 4686$  (*bottom right*) for this large change in continuum state. We emphasize that the major changes in responsivity with radius are not a result of our choice of fixed-column density clouds; this is discussed below. The dashed and dotted curves represent the responsivities for small changes in

the continuum flux about the high and low continuum states, respectively, and these are discussed in § 3.1 and § 3.3. It is clear from the global responsivities that larger relative variations of these emission lines’ surface fluxes due to changes in the continuum state can be expected to occur at larger radii where the incident continuum fluxes are smaller.

We can understand the general trends in line responsivity, with a minimum number of model dependent assumptions, through a study of Figure 1. We can relate the responsivity to the gradient in the EW contours in Figure 1 as

$$\frac{d \log F_{line}}{d \log \Phi_H} = \eta = \frac{d \log EW}{d \log \Phi_H} + 1. \quad (2)$$

The responsivity is proportional to the efficiency in converting a *change* in the number of ionizing continuum photons into escaping line photons, and so is in proportion to the change in EW contours shown in Figure 1 relative to the incident photon flux. For a fixed scale in cloud distance from the central ionizing source, the EW contours in Figure 1 shift vertically upward with a decrease in the continuum luminosity, and shift vertically downward with an increase in the continuum luminosity. Clouds in the density-flux plane for which the line EW distribution is either flat or changes little with the incident photon flux have responsivities that lie near 1 (i.e., roughly 1:1 line:continuum variations) for that line (see, especially,  $He\ II\ \lambda 4686$ ). Those clouds whose line EWs increase with increasing incident photon flux have responsivities exceeding 1 for that line (bottoms of the panels for each of these lines except  $Ly\alpha$ ). Those clouds whose line EWs decrease with increasing incident photon flux have responsivities less than 1 for that line: the steeper the gradient, the lower the responsivity. Finally, where the line EWs decline very rapidly with incident photon flux in the density-flux plane (near the central diagonal of the figures), the emission line responsivities become negative.

To illustrate these effects, in Figure 4 we superpose a responsivity grey-scale on the EW contours for each of the lines in Figure 1. The grey-scale representations are:  $\eta < 0$  (*white*),  $0 \leq \eta < 0.5$  (*light gray*),  $0.5 \leq \eta < 1.0$  (*medium gray*),  $1.0 \leq \eta < 1.5$  (*medium dark gray*),  $1.5 \leq \eta < 2$  (*dark gray*), and  $\eta \geq 2$  (*black*, appears only in  $He\ II$ ).

<sup>3</sup>In an alternative approach to analyzing the emission-line response to continuum variations, Sparke (1993) compared the width of the emission-line ACF with that of the continuum ACF.

Given that we generally measure  $0 < \eta_{eff} < 1$  for the broad emission lines, this diagram shows how the emissivity and responsivity together constrain the cloud properties, especially their distribution in radius from the continuum source.

We now briefly describe how the responsivities of the optical recombination lines arise. At sufficiently high gas densities and ionizing photon fluxes, each of these four emission lines' EWs diminish with increasing value of the ionizing photon flux (Fig. 1). This indicates a lessening efficiency of the conversion of ionizing continuum photons to escaping line photons for those clouds lying nearer to the continuum source. This is primarily due to the increasing populations and thus optical depths in the excited states of hydrogen and helium with increasing continuum flux (Netzer 1975; Netzer 1978; Ferland & Netzer 1979; Ferland, Netzer, & Shields 1979; Kwan 1984; Rees, Netzer, & Ferland 1989; Ferland et al. 1992; Shields & Ferland 1993), i.e., thermalization at large optical depth. At a given continuum flux, the optical depth of H $\alpha$  is largest, followed by H $\beta$ , He I  $\lambda$ 5876, and He II  $\lambda$ 4686 (Rees et al. 1989). Various background opacities also play a role (Shields & Ferland 1993), and photoionization out of excited states of hydrogen becomes effective for densities exceeding  $\sim 10^{10} \text{ cm}^{-3}$ . In fact, those high density clouds lying above roughly the  $\text{EW}(\text{H}\alpha) = 5 \text{ \AA}$  contour (0.7 dex) in Figure 1 lack a hydrogen ionization front for this reason. As a consequence of these optical depth effects, the more substantial relative flux variations in these four emission lines tend to be weighted by clouds lying at larger radii. This latter point should be true to some extent for most emission lines, since they too suffer from diminished efficiency in the conversion of ionizing continuum photons into escaping line photons at smaller radii where the gas densities of clouds that emit the lines must be higher. Refer to Figure 2 of KG00 for the EW contours in the density-flux plane for the stronger UV emission lines. The Mg II  $\lambda$ 2800 emission line is most like the Balmer lines in this respect, and we would expect that line to have a similarly low responsivity (see Figure 2b in KG00). This is indeed generally observed (e.g., see Clavel et al. 1991). Clouds fully ionized in hydrogen (such as those lying near or within the rapidly declining EW contours running diagonally in the density-flux planes in Figure 1),

with their very low ( $\sim 0$ ) or even negative responsivities, might in principle be arranged in such a way as to substantially reduce the line responsivity at the larger radii. However, these low efficiency clouds will not contribute much light and therefore will add little to the integrated line response unless their covering fractions are very large.

For time-scales of the order of the light-travel time across the BLR, the power spectrum of the continuum fluctuations coupled with light-travel time effects across a finite geometry will also factor into the variations of an emission line's flux and perhaps profile. However, *it is the responsivity that establishes the outer envelope of these variations*. Light travel time effects can only act to reduce or dilute the observed line response. We reiterate that the variations in the line intensity ratios and line profiles presented here are *not* due to light travel time effects (e.g., see Robinson, Pérez, & Binette 1990; Pérez, Robinson, & de la Fuente 1992; Pogge & Peterson 1992) or other geometrical effects (e.g., line anisotropy, O'Brien, Goad, & Gondhalekar 1994), but are rather due to differences in the time-averaged photon flux incident on a spatially extended BLR and their effect on the line emissivity. Krolik et al. (1991), Pogge & Peterson (1992), and Gilbert & Peterson (2003) have found that reverberation effects on the  $L_{line} \propto L_{cont}^\eta$  relation can be largely removed by correcting the emission-line light-curves for their mean time-delays. If this is indeed the case, then any residual line – continuum flux correlations must be primarily due to the responsivity of the gas in the BLR, as we have defined here. However, if a line's transfer function has a long tail in time delay (in comparison to the important continuum variability time scales), simply removing the lag may not sufficiently correct for this geometric dilution of the line response. The observed lag-corrected emission-line response will then be a function of the line's responsivity, as defined here, and the prior continuum history. More advanced methods, such as that introduced by Horne et al. (2003), may then be needed to disentangle the effects.

Finally, it is apparent from Figs. 1, 3, and 4 that He II  $\lambda$ 4686 should be the most responsive emission line of the four optical emission lines discussed here, followed by He I, H $\beta$ , and lastly H $\alpha$ . This is observed (e.g., see Wamsteker et al. 1990; Diet-

rich et al. 1993; Kollatschny 2003). The model effective global responsivities of these four emission lines are listed in column (2) of Table 1. To illustrate the trends within the Balmer line series, we also plot the EW distribution of  $H\gamma$   $\lambda 4340$  within the density-flux plane in Figure 1, list its effective responsivity in Table 1, and illustrate its responsivity in the density-flux plane in Figure 4.  $Ly\alpha$   $\lambda 1216$  is also a recombination line, but with different physics, and so we provide the same information for it.

### 3.1. The Emission-Line Response Versus the Local Ionizing Photon Flux and Continuum Luminosity State

Figure 3 shows that the responsivity of  $H\beta$  is expected to be a strong function of radius, varying from  $\sim 0.2$  in the inner BLR to  $\sim 1$  at the outer radius. More generally, this is indicated by the gradient in the EW contours with respect to the ionizing photon flux in Figure 1 (see also Eq. 2), and coarsely illustrated in Figure 4. Another interesting point raised by Figure 3 is that the  $H\beta$  line response should be significantly stronger during low continuum flux states than during high ones for similar continuum fluctuation amplitudes. This is illustrated in Figure 3 by the dotted and dashed curves representing the low and high continuum state  $H\beta$  line responsivity, respectively, computed for small (0.1 dex) variations about the high and low states. The effective responsivities in the high and low states are given in columns (3) and (4) of Table 1. K. Horne (2002, private communication, and 2004, in preparation) recovered the luminosity-dependent delay map for the 13 yr monitoring campaign of the  $H\beta$  broad emission line of NGC 5548, and found a similar relation between the amplitude of the line response with continuum state.

Figure 3 and columns (3) and (4) of Table 1 shows that all of these lines display generally larger effective responsivities at larger distances (lower incident photon fluxes) and during lower continuum states. Additionally, the amplitude of the change in effective responsivity with continuum state differs substantially between the Balmer and helium lines, and this should be diagnostic of the physical conditions within the BLR. By contrast,  $Ly\alpha$  shows very little variation in responsivity with cloud parameters (Fig. 4), and as a conse-

quence shows a very modest change in  $\eta_{eff}$  with continuum state (Table 1).

We elucidate the change in the radial responsivity with continuum state shown in Figure 3, using He II  $\lambda 4686$  by way of example. In both continuum states, the responsivity at large radii is nearly independent of radius and continuum state. This is simply a reflection of the general lack of dependence of the line EW with incident continuum flux for  $\Phi_H \lesssim 20.5$  (see Figure 4). This is in contrast to the case of the Balmer lines, especially  $H\alpha$ . Note also in Figure 4 that most of the variations of  $\eta(\text{He II})$  with incident photon flux occur for  $\Phi_H \gtrsim 20.5$ ; here in particular  $\eta$  declines with increasing  $\Phi_H$ . This dependence of the responsivity on incident continuum flux makes this line’s radial responsivity at small distances quite dependent on the continuum state as well. These effects are also illustrated in Figure 3. The “knee” in the radial responsivity of He II occurs at the radius corresponding to  $\Phi_H \approx 20.5$  for each continuum state, or  $\log r \approx 16.25$  (7 lt-days) in the mean continuum state. Simply put, strong anti-correlations between the line EW and the incident photon flux will correspond to anti-correlations between  $\eta$  and the incident photon flux, which in turn will result in similar anti-correlations between  $\eta$  and the continuum state. Likewise,  $\eta_{eff}$  will anti-correlate with the continuum state, as weighted by the line’s radial luminosity function. Based on single power-law cloud distribution models, O’Brien, Goad, & Gondhalekar (1995) also found “a decrease in the mean response when the continuum flux increases.”

By definition, a time-varying responsivity  $\eta(r, L_{cont}(t))$  implies that the line transfer function,  $\Psi(\tau, v)$ , is time-dependent (i.e., non-stationary). In this case the time dependence is due to changes in the time-averaged photon flux incident on a spatially extended BLR. We therefore expect the measured lags of the emission lines and their profile shapes to depend on the luminosity state of the continuum (§ 3.3 & § 3.4). We note that unless the velocity field is self-similar in radius (Goad et al. 1999), a profile shape that depends on the continuum luminosity state fails a hysteresis test (see Wanders 1994; Perry, van Groningen, & Wanders 1994). This is true without invoking a redistribution of material within the BLR or other geometrical effects as suggested by Wanders

& Peterson (1996).

### 3.2. The Intrinsic Baldwin Effect

Detailed analyses of the AGN broad emission-line response to continuum variations in spectrophotometric monitoring campaigns show that in all cases the responsivity in most measured lines is  $< 1$ , even after accounting for light travel-time effects (e.g., Krolik et al. 1991). Referring to Eq. 2, we see that this requires the line equivalent width to diminish with increasing continuum flux and vice versa: the intrinsic Baldwin effect ( $EW_{line} \propto L_{cont}^\beta$ ; see Kinney, Rivolo, & Koratkar 1990; Krolik et al. 1991; Pogge & Peterson 1992; Peterson 1997; Gilbert & Peterson 2003). In concurrence with Gilbert & Peterson the present work suggests that the origin of the intrinsic Baldwin effect is due either in whole or in large part to the line’s responsivity being less than 1 throughout the majority of a distribution of largely ionization-bounded clouds (as shown in Figure 1), i.e., without the *necessity* of a large population of matter-bounded clouds (Shields, Ferland, & Peterson 1995), although we do not rule these out. As discussed above we expect  $\eta_{eff} < 1$  for most lines, and thus most lines should demonstrate an intrinsic Baldwin Effect, since the intrinsic Baldwin effect index  $\beta$  is related to the responsivity as  $\beta = \eta_{eff} - 1$ . Based on single power law cloud distribution models, O’Brien, Goad, & Gondhalekar (1995) showed that an intrinsic Baldwin effect can be induced in any line by changing its responsivity with continuum level. While we concur with these findings, we find a more general and significant origin for this effect, namely  $\eta_{eff} < 1$  as defined and described in § 3.

Our simple model for the BLR of NGC 5548 predicts an  $\eta_{eff}$  for  $H\beta$  of 0.54 in the 1989 high state and 0.77 in the 1992 low state (columns (2) – (4), Table 1). That is, we expect  $\eta_{eff}$  and so the slope in the intrinsic Baldwin effect to be a function of continuum state. Compare the dotted and dashed lines in Figure 3. This predicted range in  $\eta_{eff}$  approximately brackets that measured in the same object by Gilbert & Peterson (2003) of 0.53 – 0.65.<sup>4</sup> A line’s equivalent width is usually

measured with respect to the local continuum, and Gilbert & Peterson (2003) found that the underlying continuum becomes bluer when brighter in this object, such that  $L_{5100} \propto L_{1350}^{0.67}$ . They then suggested that since the  $\lambda 1350$  continuum lies closer to the ionizing continuum, it might be better to reference the  $H\beta$  flux to it, and found the relation  $L(H\beta) \propto L_{1350}^{(0.35-0.43)}$ . Our simulations assumed that the SED remains constant as its amplitude changes. Thus, while it is difficult to make detailed comparisons, we expect that SED changes are a secondary effect on the line responsivity; we discuss the impact of a variable SED on line responsivity in § 4.2. The point remains that line responsivity, as defined here, is likely to be responsible for much of the observed intrinsic Baldwin Effect.

What can the intrinsic Baldwin effect tell us about the BLR? Because the EW contours of the Balmer lines in particular in Figure 1 are so nearly proportional to the incident continuum flux, we suggest that measurements of the responsivities of these emission lines will point to the distribution of the optical recombination line-emitting entities in the density-flux plane. Low density gas ( $n_H < 10^{10} \text{ cm}^{-3}$ ) illuminated by low values of the ionizing photon flux ( $\Phi_H < 10^{18} \text{ cm}^{-2}\text{s}^{-1}$ ), and gas at any density illuminated by even lower values of  $\Phi_H$  ( $< 10^{17.5}$ ) will emit these optical recombination lines, but they *will not respond appropriately* to variations in the ionizing continuum. The responsivities of these clouds in these lines are  $\sim 1$  and  $> 1$ , respectively. Such models would fall far short of reproducing the observed variations in  $H\beta$ , *independent* of any considerations of the line luminosity or lag. Next, the observed mean responsivity of the optical He II  $\lambda 4686$  line,  $\eta \sim 0.9$  (see, for example, Dietrich et al. 1993; also Krolik et al. 1991), necessarily implies that a significant fraction of this line forms in gas exposed to high incident ionizing continuum fluxes on average ( $\log \Phi_H \gtrsim 20.5 \text{ cm}^{-2} \text{ s}^{-1}$ , or  $R \lesssim 7$  light days in NGC 5548), as well as relatively high densities<sup>5</sup>. This is just as its measured lag indicates (Clavel et al. 1991; K95). Thus, Figures 3 and 4 predict

---

obtained when this background light was allowed to vary in the fit.

<sup>4</sup>The logarithmic slope 0.65 was obtained when the value of the background galactic continuum at 5100 Å was fixed to the observed value (Romanishin et al. 1995), while 0.53 was

<sup>5</sup>Higher column density clouds would allow for somewhat lower gas densities under this condition, and vice-versa (e.g., see Korista et al. 1997).

a positive correlation between the lag of each of these lines and their responsivity,  $\eta_{eff}$ , for a particular continuum state (see also Carroll 1985). So together the luminosity, lag, *and* responsivity (intrinsic Baldwin Effect) of each of the broad emission lines for a range of continuum states should constrain the distribution of BLR cloud properties in gas density, distance from the ionizing continuum source, and column density. The quasar tomography method of Horne et al. (2003) is particularly well suited to this task, and we discuss this further in § 4.3.

### 3.3. The “Breathing” Broad Line Region

Netzer & Maoz (1990) reported that different lags for the broad emission lines of Ly $\alpha$  and C IV were found for each of the three continuum variability events during the 1989 campaign of NGC 5548 (Clavel et al. 1991). Based on data from an earlier optical campaign (Netzer et al. 1990), Netzer & Maoz also reported a significantly different lag for H $\beta$  than did Peterson et al. (1991). While acknowledging that a variable continuum ACF will change the lag, Netzer & Maoz (1990) suggested that at least part of the origin of these time-dependent lags lay in a non-linear emission-line response. Over the full 13 yr monitoring campaign of NGC 5548 Peterson et al. (2002; see also Peterson et al. 1999) found that the H $\beta$  emission-line lag scales with the mean continuum level, such that  $\tau \propto F_{5100}^{0.95}$ , albeit with much scatter. This positively correlated behavior of the lag with continuum state has been called “breathing.” After positing that the UV continuum is more intimately connected to the driving ionizing continuum and accounting for the relation they found that between the  $\lambda 5100$  and  $\lambda 1350$  continuum bands ( $F_{5100} \propto F_{1350}^{0.56}$ ), the relation  $\tau \propto F_{UV}^{0.53}$  resulted. Peterson et al. (2002) then proposed that  $\tau \propto F_{cont}^{0.5}$  might be a natural consequence of a simple ionization parameter-type argument that  $r \propto L_{ion}^{0.5}$ . Horne (2004), too, has found evidence of breathing in his transfer function analysis of the 13 yr spectroscopic dataset of Peterson et al. (2002). A breathing BLR has also been proposed by Goad et al. (1999) to explain line profile variation differences between C IV and Mg II in NGC 3516. In this subsection, we address a likely origin of breathing BLRs and comment on the conclusions drawn by Peterson et al. (2002) in regards to this

issue.

The single power law cloud distribution models of O’Brien, Goad, & Gondhalekar (1995) predicted a relation between line lag and incident continuum level (for a fixed SED) due to a non-linear emission-line response. The results presented here for the optical recombination lines based on more general models arrive at the same conclusion. The shift in the lag as a function of the continuum state is a reflection of an outward shift in the line’s luminosity-weighted radius to gas at larger radii that is better able to reprocess the increased continuum luminosity into line emission, and vice versa in low continuum states. The EW contours in Figs. 1 and 4 shift vertically as the source luminosity changes, causing corresponding changes in the radial responsivity and hence responsivity-weighted radii. We therefore expect that elevated continuum states will be accompanied by an increase in the line lag and a decrease in the line responsivity.

Breathing will not occur for lines for which the responsivity as a function of radius and ionizing continuum level is constant. A constant  $\eta(r, L(t))$  implies that the emissivity-weighted and responsivity-weighted radii are the same (see Goad et al. 1993), and therefore the measured lag is independent of the continuum state. Therefore, if after correcting for reverberation effects, the measured lag varies with luminosity, then so must its effective responsivity. Although Gilbert & Peterson (2003) did not note any evidence for changes in  $\eta_{eff}$  with continuum level, B. Peterson (2003, private communication) finds that a detailed analysis of the 13 yr campaign on a year-to-year basis indicates changes in the line–continuum flux slope. It is also significant that while BLRs whose lines breathe must show an intrinsic Baldwin effect for those lines, the converse is not true. For example, for the case of  $\eta = 0.5$  everywhere, no breathing will occur, but an intrinsic Baldwin effect will be present.

The two triangles in each panel of Figure 3 mark the positions of the responsivity-weighted radii ( $R_\eta$ ) of H $\beta$  and the other three emission lines for the two continuum states. In the case of H $\beta$ , it is larger in the high continuum state by a factor of  $\sim 1.6$  relative to the low state. This is about the same ratio of luminosity dependent lags observed in this line in NGC 5548 for the same two



continuum states ( $\sim 1.7$ ; Peterson et al. 2002; see also Wanders & Peterson 1996; K. Horne 2004, in preparation), although we note that the measured lag is expected to be smaller than  $R_\eta/c$  by a factor of a few (e.g., see Pérez et al. 1992).

The effective line responsivities for the high and low continuum state are given in columns (3) and (4) of Table 1. As discussed in § 3.1, the low-state responsivity is higher in every case, and Figure 3 shows that the line effective responsivity and  $R_\eta$  shift to larger distances in higher continuum states. For this particular model, the responsivity-weighted radius scales as  $R_\eta \propto L_{cont}^\gamma$ , with  $\gamma = 0.15, 0.23, 0.38,$  and  $0.44$  for  $H\alpha, H\beta, He I,$  and  $He II,$  respectively. These relations should be diagnostic of the physical conditions within the BLR. The general relation proposed by Peterson et al. (2002), above ( $\gamma = 0.5$ ), is expected to hold only if the line responsivity is constant over a large portion of the BLR with a steep break to lower responsivity (see for example, He II in Figure 3), and so is not the general case. The breathing amplitude (e.g., the value of  $\gamma$ ) is expected to depend on the responsivity and the extent to which the responsivity changes with both radius and continuum state in the vicinity of  $R_\eta$  (compare dotted and dashed curves for each of the lines in Figure 3). Using the relation between the  $\lambda 5100$  and  $\lambda 1350$  continuum fluxes for NGC 5548 (Gilbert & Peterson 2003; but see also Peterson et al. for a slightly different value), and assuming that  $L_{1350}$  is a proxy for the driving continuum, K. Horne (2002, private communication, and 2004, in preparation) finds a similarly weaker relation between the  $H\beta$  lag and continuum luminosity state for the 13 yr campaign of NGC 5548 as do we. In addition, since  $\gamma$  is related to the responsivity, it too changes with continuum level (see also O’Brien et al. 1995).

Finally, we note that the expected larger line response during low continuum states (§ 3.1) will be enhanced by the fact that an effectively smaller line-emitting region, due to this breathing, respond more coherently to a given continuum variation. The opposite hold for variations about high continuum states. The combined effect can be investigated in data sets such as the 13 yr  $H\beta$  light curve presented in Peterson et al. (2002; their Figure 1): more coherent and larger amplitude responses in  $H\beta$  should generally be found at low

continuum states, while just the opposite should result during high continuum states. One might also find differences in line responsivity between two comparably low continuum states that immediately straddle a high continuum state in time, due to light travel time effects that are not removed from the second low state by simply correcting for the lag.

### 3.4. Integrated Line Flux Ratios vs. Continuum State

In this section, we investigate the expected changes in the integrated line flux ratios due to changes in the continuum state. It should now be apparent that such line ratio variations will result simply because the responsivities differ between the emission lines. Lines with greater responsivities vary with greater amplitudes with changing continuum state, and so line flux ratios can be expected to change as well. Other factors may play a role, but responsivity effects will be present regardless.

Figure 5 illustrates the  $H\alpha/H\beta$  line flux ratio varying across the density-flux plane, from roughly 17 (near the triangle at the bottom) to approximately 1 (near coordinates: [13.5, 22.5]). The classical nebular theory of hydrogen Balmer lines (Menzel case B ) does not apply to the gas occupying the BLR. For example, at coordinate [12.0, 19.5] in the density-flux plane (corresponding to a distance of 22 lt-days in the mean continuum state), case B predicts  $H\alpha$  and  $H\beta$  fluxes that are  $20.8\times$  and  $30.4\times$  larger than that emitted by the cloud. The case B  $H\alpha/H\beta$  flux ratio is 2.35, whereas the ratio predicted by Cloudy is 3.44. Over a significant portion of the density-flux plane *this ratio is inversely proportional to the incident continuum flux*, as expected from the optical depth effects mentioned earlier, and in agreement with the findings of Rees, Netzer, & Ferland (1989; see also Netzer 1975). This being the case, it is easy to imagine this ratio changing in response to variations in the incident continuum luminosity. Thus, differences in responsivity among the Balmer lines, as illustrated in Figs. 1, 3, 4 and as listed in Table 1, probably account for most of the observed steepening in the broad-line Balmer decrement as the continuum drops into low states, and flattening in high states. There have been many such broad line Balmer

decrement/continuum state correlations reported in the spectra of variable Seyfert 1 galaxies (see, for example, Antonucci & Cohen 1983; Ferland, Korista, & Peterson 1990; Wamsteker et al. 1990; Tran, Osterbrock, & Martel 1992). Integrated over this model’s full broad line-emitting region, the  $H\alpha/H\beta$  flux ratio changes from 4.9 in the low state to 3.7 in the high state. While the particulars are model dependent, the trend generally is not. The Balmer decrement’s variations with the incident continuum level should be sensitive to the distribution of clouds in the density-flux plane. Furthermore, we suggest that a Seyfert 1 galaxy’s sub-classification as Seyfert 1.0, 1.5, 1.8, or 1.9 (as defined in Osterbrock 1989, and references therein) may at least in part be due to the relative flux of ionizing photons present within their broad-line regions at the time of observation. That is, any given spectrum of a Seyfert Type 1 AGN may pass through some of these sub-classifications as its continuum luminosity fluctuates from high (Seyfert 1 or 1.5) to low continuum states (Seyfert 1.8 or 1.9). In high continuum luminosity states, a larger broad-line contribution to the total (broad + narrow) Balmer line profile will be present and the broad Balmer line decrement will be flatter. In low continuum luminosity states, the broad-line contribution to the total Balmer line profile will be relatively much smaller, and the broad Balmer line decrement will be steeper. NGC 5548 is generally classified as Seyfert 1.5. However, the order-of-magnitude continuum fluctuations that occurred over the 13 yr optical monitoring campaign (Peterson et al. 2002) probably drove the Balmer emission-line spectrum from Seyfert type 1.8 in 1992 to perhaps Seyfert type 1.0 in 1998.

As described above, the Balmer lines should show less flux variation with continuum state than He I, which in turn should show less variation than He II. This trend is generally observed (Peterson & Ferland 1986; Ferland, Korista, & Peterson 1990; Wamsteker et al. 1990; Dietrich et al. 1993; Peterson et al. 1993; Kollatschny 2003). Particularly interesting is that observed changes in the  $H\beta/He\ II$  flux ratio may, at least in part, be due to *differences in the way these two lines respond to the level of the ionizing continuum flux*, rather than to changes in the shape of the ionizing SED. For the model presented here, this ratio drops by

nearly a factor of 2 from the low to high continuum states. To a lesser extent, this is likewise true for the He II/He I line ratio, which changes by a factor of 1.3. Such a responsivity effect may have played a role in the observation of a large increase in the He II  $\lambda 4686$  equivalent width in comparison to  $H\beta$  during a large increase in the continuum luminosity in NGC 5548 (Peterson & Ferland 1986) and likewise in a similar event reported by Peterson et al. (2000) in NGC 4051. While the broad line He II/ $H\beta$  flux ratio is sensitive to the ionizing SED, the usual photon-counting (Zanstra) argument used to measure the 13.6 to 54.4 eV continuum SED applies strictly when these lines are emitted in gas whose properties allow for responsivities  $\eta_{eff} \approx 1$ , as would be true if case B applied for both lines. However, these conditions *do not* apply for the Balmer lines emitted within the BLR, but they can be found within the narrow line regions of AGNs (see the EW distributions of the recombination lines in Ferguson et al. 1997) or within galactic nebulae. On the other hand, the He II emissivity does not stray too far from that expected from case B for most conditions expected in the BLR, as indicated by its comparatively featureless EW distribution in the density-flux plane for  $\log \Phi_H \lesssim 21$  (see also Bottorff et al. 2002).

Finally, as a matter of general interest we note that the  $Ly\alpha/H\beta$  flux ratio should correlate with the continuum flux, and apparently this is the case in the well-studied AGN NGC 5548 (Wamsteker et al. 1990). The EW contours of  $Ly\alpha$  in the density-flux plane (see Figure 1, *bottom right*) do not show as strong continuum flux dependencies as do the Balmer lines, and so  $\eta(Ly\alpha) > \eta(H\beta)$  can be expected, with larger differences to come from gas nearer to the continuum source where the responsivity of  $H\beta$  is small (see also Figure 4). The combined conclusions of Pogge & Peterson (1992) and Gilbert & Peterson (2003) would indicate an observed relation of  $L(Ly\alpha)/L(H\beta) \propto L_{1350}^{0.12-0.24}$  in NGC 5548. Our simple model (see Table 1) predicts a similar relation  $L(Ly\alpha)/L(H\beta) \propto L_{1350}^{0.10}$ , which is steeper in high continuum states and shallower in low ones. Shields & Ferland (1993) discussed some of the mechanisms behind the destruction of  $Ly\alpha$  emitted by broad-line clouds. Pogge & Peterson also found that in Fairall 9  $\eta_{eff}(Ly\alpha) \approx 0.71$  for a factor of  $\sim 10$  change in the observed  $\lambda 1338$  continuum, similar to the value re-

ported here (0.74, Table 1) for our simple model. Figure 4 shows that  $\eta(\text{Ly}\alpha)$  is nearly independent of gas density and incident photon flux over a wide range in these parameters.

### 3.5. Line Profiles and Their Variations with Continuum State

While the dynamics of the gas emitting the broad emission lines are not yet understood, the importance of a virial component seems to be reasonably well established (Peterson & Wandel 2000). Here, we have adopted the simple relationship

$$v(r) = (GM/r)^{1/2}, \quad (3)$$

assuming randomly inclined circular orbits and a central mass of  $8.3 \times 10^7$  solar masses, chosen to approximately reproduce the observed broad-line FWHM of  $\text{H}\beta$  in NGC 5548. This choice of dynamical model is motivated by simplicity for purposes of demonstration.

The low-state continuum emission-line profiles of the four lines under study, as predicted by our simple LOC model line emissivity and velocity field, are shown in Figure 6, normalized to their peak intensities. We note that the flat tops to these profiles are artifacts of the assumption of circular orbits, and their extents are determined by the local Keplerian velocity at the distance of the model's outer radius (140 lt-days) given the assumed central mass. The EW distributions shown in Figure 1, and most notably the continuum flux at the onset of significant thermalization, are roughly reflected in the widths of the emission-line profiles in Figure 6, as well as in their observed lags (Dietrich et al. 1993; Peterson & Wandel 1999, 2000; Fromerth & Melia 2000). He II is the broadest line (with the shortest lag), followed by He I, then  $\text{H}\beta$ , and finally  $\text{H}\alpha$  (with the longest lag). This is as generally observed in broad-line AGNs (Stirpe 1990, 1991; Crenshaw 1986, Shuder 1982, 1984; Osterbrock & Shuder 1982; Boroson & Green 1992; Kollatschny 2003). Krolik et al. (1991), Peterson & Wandel (1999, 2000), and Onken & Peterson (2002) present highly correlated lag – line width relations that indicate virial-like motions in the vicinity of a supermassive central object. The FWHM of these four emission lines, as well as  $\text{H}\gamma$  and  $\text{Ly}\alpha$ , are listed in columns (5) and (6) of Table 1 for the

high and low continuum states, respectively. The trend in line widths is in general agreement with those found in the models presented by Rees, Netzer, & Ferland (1989).

Since the lines under study here are recombination lines involving just one or two electrons, they are emissive over very broad areas within the density-flux plane, unlike the collisionally excited metal lines which are very sensitive to the ionization parameter. The Balmer and He I lines span essentially equal areas of significant emissivity within the density-flux plane *without regard to ionization parameter*, and that of He II does likewise for  $\log U_H \gtrsim -3.5$  (see Figure 1). While it is also true that a cloud of a given column density will become fully  $\text{He}^{++}$  at a higher ionization parameter than for  $\text{H}^+$ , this difference is small (see Figure 1). By far most of the differences in emissivity among the Balmer and He I lines are due to the optical depth effects discussed above, and this is also true for the He II lines except for clouds with  $\log U_H \lesssim -3.5$ . Stated another way, if all of these lines were emitted with their case B emissivities within the BLR, much smaller differences in their profiles and lags would be expected.

Figure 7 shows the long term (global) responsiveness for each of the four emission lines as a function of radial velocity across their line profiles, for our simple velocity field. Because of the larger response in the line cores, the broad emission-line component of the Balmer lines should become narrower/peakier in higher continuum states, and broader/less peaky during low continuum states (cf.,  $\text{H}\alpha$  variations in NGC 5548; Stirpe et al. 1988); refer also to the model high and low continuum state FWHMs as listed in columns (5) and (6) in Table 1. In fact for this particular model, a continuum state that is a factor of  $12\times$  brighter than the low state<sup>6</sup> produces a FWHM in  $\text{H}\beta$  that is  $1000 \text{ km s}^{-1}$  narrower than that in the low state. The response across the profile of He II is *much higher*, although again this emission line would be expected to be somewhat narrower during higher continuum states. The response across the profile of He I is not as broad as He II and not as peaky as the Balmer lines. In every case, *we ex-*

<sup>6</sup>Such a high state in NGC 5548 was recorded in 1984 (Wamsteker et al. 1990) and again in 1998 (Peterson et al. 2002).

pect the response in the line cores to be stronger than in the line wings. The relative change in the FWHM of the emission line with continuum state is effectively a reflection of the “breathing” BLR as caused by changes in the line responsivity, as we discussed in § 3.3. O’Brien, Goad, & Gondhalekar (1995) similarly linked non-linear emission-line response to line profile variability, although this general conclusion was based on single power law cloud models.

### 3.6. Radial Velocity-Dependent Emission-Line Ratios and Their Variations with Continuum State

Since the responsivity of these lines is expected to be radially dependent and this function differs between emission-line species, we expect radial velocity-dependent variations in the line intensity ratios. These effects are illustrated in Figure 8, which shows the velocity-dependent Balmer decrement ( $H\alpha/H\beta$ ) for the low-state (*dotted line*) and high-state (*solid line*) continuum. Note that in both cases the Balmer decrement is steeper in the line core than in the line wings, and the Balmer decrement shows larger changes with continuum level in the line core (from 5.6 to 4.0), than in the line wings (from 3.0 to 2.7). The first of these effects has been well-established (see, for example, Shuder 1982, 1984; Osterbrock & Shuder 1982; van Groningen 1984, 1987; Crenshaw 1986; Stirpe 1990, 1991; Kollatschny 2003), and we are aware of just one study of the time-dependent variability of the Balmer decrement as a function of radial velocity (Stirpe, de Bruyn, & van Groningen 1988). Both behaviors imply that *the velocity field must decrease with increasing radius from the central source*. As just presented above, a weaker response in an individual line’s wings in comparison to its core (Fig. 7) would also argue for such a velocity field. These findings are consistent with recent reverberation studies that find a relationship between the emission-line lag and rms profile width for multiple lines in individual AGNs, which implies that the velocity field is dominated by the central massive object (Peterson & Wandel 1999, 2000; Fromerth & Melia 2000).

The results presented here also predict a smaller  $H\beta/He\ I$  intensity ratio in the line wings than in the core (Fig. 8). The EW contours in Figure 1 coupled with a velocity field that diminishes with

increasing distance from the central source provide possible explanations for this generally observed phenomenon (Shuder 1982, 1984; Osterbrock & Shuder 1982; Crenshaw 1986; van Groningen 1984, 1987; Rees, Netzer, & Ferland 1989; Kollatschny 2003). These lines’ EWs peak up at similarly high densities, but the He I line peaks up at significantly higher photon fluxes (smaller radii), because of its lower optical depth. This is responsible for this line’s relatively stronger wings (see also Netzer 1978; Kwan 1984; Carroll 1985; Carroll & Kwan 1985).

Whether or not the specific dependencies of the continuum state/responsivity effects described in this section are present in the spectra of NGC 5548 or other variable Seyfert 1 AGNs is not particularly important. We discuss the sensitivity of line responsivity to model assumptions in the Appendix. Instead, the emphasis of this paper lies mainly in illuminating the mostly untapped wealth of the potentially powerful physical diagnostics present in high quality spectrophotometric data sets of the optical recombination lines, and that their emissivities’ sensitivity to the continuum flux makes them particularly effective diagnostics of the radially dependent physical conditions within the BLR.

## 4. DISCUSSION

### 4.1. Optically Thin Gas in the So-Called Very Broad Line Region

That the BLR may contain a significant component of ionized gas that is optically thin to hydrogen-ionizing photons has been suggested by investigators over many years. In nearly every case there is an association of this gas with that emitting the very broad wings of the lines. Most recently, Sulentic et al. (2000) reported that in the quasar PG 1416–129 the FWHM of the broad emission-line profile of  $H\beta$  increased by 50% from a high to a low continuum state separated in time by 10 yr. Their interpretation of this is that the wings of the Balmer lines are dominated by emission from an optically thin “very broad line region” (VBLR), while the core of the line is dominated by more highly variable optically thick gas. These are usually thought of as two distinct line-emitting regions. Ferland, Korista, & Peterson (1990), Peterson et al. (1993), and Corbin & Smith (2000)

made similar arguments based on Balmer line – continuum variations, while Gondhalekar (1987, 1990), O’Brien, Zheng, & Wilson (1989), & Pérez, Penston, & Moles (1989) found less variable wings in Ly $\alpha$  and C IV  $\lambda$ 1549 of higher redshift quasars. Kassebaum et al. (1997) found similarly stronger variations in the line core than wings of H $\beta$  in Mrk 335. It should be noted that while the conclusions regarding the core versus wing variations from monitoring campaign studies such as Peterson et al. (1993) and Kassebaum et al. (1997) were based on analyses of *time-resolved* spectral observations of the continuum and H $\beta$ , most of the above studies relied on very few, often just two, observation epochs. Without sufficient time resolution of the variability, it is difficult to assess the actual line response. Additional arguments for an optically thin line-emitting region have been put forth through the analyses of line flux ratios in the profile wings: optical Balmer and He II lines (Marziani & Sulentic 1993; Corbin 1997), Balmer and C IV  $\lambda$ 1549 (Corbin 1995), Balmer and Ly $\alpha$  line profiles (Zheng 1992), and Balmer and O I  $\lambda$ 8446 profiles (Morris & Ward 1989).

While at any given continuum state the broad emission-line region may well contain clouds fully ionized in hydrogen, as the present model does, the results presented here suggest that there is no great need for a major line-emitting component consisting of vast amounts of optically thin gas. Most of the effects mentioned just above regarding the Balmer and helium recombination lines can be explained by the effects we described in § 3: weak Balmer line emission and response need not originate in clouds optically thin to the Lyman continuum. While an emission line such as Ne VIII  $\lambda$ 774 is likely to be emitted mainly within clouds that lack a hydrogen ionization front (e.g., see Hamann et al. 1998; Korista et al. 1997), we have also pointed out that by their very nature fully-ionized clouds are inefficient emitters of hydrogen recombination lines (refer again to Figure 1), and so are unlikely to be important energetically even if their covering fraction is large. This is especially true in the face of a variable ionizing continuum source; clouds will more likely be either ionization-bounded or too overionized to emit Balmer lines of any significance. It is also significant that the matter-bounded clouds in Fig-

ure 4 either have small positive (*lightest gray*)<sup>7</sup> or negative (white) responsivities. Even if present, the latter type clouds never make their presence known in these emission lines, which is not surprising given their extremely low emitting efficiencies.

In regards to the comparisons of Balmer and Ly $\alpha$  line profiles, as mentioned in § 3.4, the EW contours of Ly $\alpha$  in the density-flux plane (see Figure 1, *bottom right*) do not show the strong continuum flux dependencies of the Balmer lines. We suspect that this, along with the presence of a radially decreasing velocity field, accounts for the very large Ly $\alpha$ /H $\beta$  ratios found in the emission-line wings by Zheng (1992), rather than these ratios being due to a major constituent of optically thin emitting gas.

Finally, we also point out that many of the above studies assumed that case B emissivities apply to the hydrogen lines emitted by optically thick clouds in the BLR and attributed significant deviations from expected ratios to an optically thin emitting region. We conclude that a separate optically thin VBLR may be unnecessary, and in any case for the Balmer lines is probably energetically unimportant. The wings of the hydrogen recombination lines likely represent nothing more than the inner BLR where the Balmer line emission is inefficient and the responsivity low.

#### 4.2. Effects of an SED that Varies with Continuum Level

Paltani & Courvoisier (1994) and Paltani & Walter (1996) showed unambiguously that the UV continuum becomes bluer when the flux is higher in variable AGNs. This effect has also been found in the Sloan Digital Sky Survey quasar sample (Vanden Berk et al. 2004). In the particular case of NGC 5548, Maoz et al. (1993) reported that, after accounting for the Balmer continuum and UV Fe II emission, the 1800–2400 Å continuum becomes bluer with increased continuum flux. Additionally, Peterson et al. (2002) and Gilbert & Peterson (2003) found that after careful removal of the contaminating non-variable stellar optical continuum flux, the UV-optical continuum in NGC 5548 becomes bluer as it becomes

<sup>7</sup>The *only* clouds in Figure 4 whose hydrogen line responsivities are  $\approx 0$  lie above the diagonal line  $\log(U_{HC}) \approx 10.25$  and also within the lightest gray shaded region.

brighter:  $F_{5100} \propto F_{1350}^{0.67}$ . Extrapolation of this relation to higher energies might indicate a hardening of the incident ionizing continuum during brighter continuum states. Marshall et al. (1997) found larger amplitude variations in the extreme ultraviolet ( $\sim 100 \text{ \AA}$ ) than at  $1350 \text{ \AA}$  during a week-long period of the 1993 NGC 5548 monitoring campaign. Alternatively, as suggested by Paltani & Walter (1996), it may indicate the presence of a constant (or more slowly varying) continuum or pseudocontinuum component whose contribution is greater at longer wavelengths. Korista & Goad (2001) found that 20%–30% of the observed effect may be due to reverberation of the diffuse continuum emission of the broad line clouds. In the simulations presented here, the SED of the continuum incident on the broad-line clouds is the same for both high and low continuum states. How an emission line’s responsivity would change with an *incident* SED that changed shape as the UV-optical continuum level varied will depend on the details of how the flux of photons important to the creation and destruction of the line varies. We briefly discuss these effects here.

The shape of the ionizing continuum determines the heating for given values of gas density, ionizing photon flux, and chemical abundances. All else being equal, harder incident continua result in higher electron temperatures, and so major cooling lines (e.g., C IV  $\lambda 1549$ ) might be expected to increase their energy output in response. One should also keep in mind that the incident flux at energies corresponding to the *Balmer* continuum is important to the destruction of hydrogen emission lines for the high gas densities encountered in the BLR (Shields & Ferland 1993). Also, harder continua during brighter UV-opt continuum states might also mean comparatively more photons above 1 ryd and/or 4 ryd, favoring the production of hydrogen and helium recombination lines. Kaspi & Netzer (1999) considered an SED whose break near 4 ryd moves to higher energies for brighter UV continuum states (their Figure 8d), with the effect of increasing the 4 ryd/1 ryd photon flux ratio with increasing  $\lambda 1350$  continuum luminosity. However, in this variable SED scheme, the flux above 20 ryd (270 eV) remained constant. A comparison of their Figs. 7 (fixed SED) and 9 (variable SED) that show their model predictions of five UV emission

lines’ light curves versus observations illustrates some of the aforementioned effects of a variable continuum SED on line responsivity. While they included He II  $\lambda 1640$  in their simulations, such was not the case for the Balmer lines. Their prescription for a variable continuum SED increased the responsivities of the He II and Ly $\alpha$  lines, whereas those of C IV  $\lambda 1549$ , C III]  $\lambda 1909$ , and Mg II  $\lambda 2800$  decreased, presumably because the variations in the continuum beyond  $\sim 150 \text{ eV}$  were smaller in their variable SED scheme than for the constant SED. It is also apparent that the lags of He II and C IV increased in the higher continuum states, because of a shift to larger responsivity-weighted radii.

### 4.3. The Importance of the Recombination Lines to the Method of Quasar Tomography

The method of “quasar tomography,” proposed by Horne et al. (2003), is a unification of reverberation mapping and photoionization physics. Its goal is to place physical constraints on the recovered two-dimensional transfer function map  $\Psi(\tau, v)$  of the broad emission lines, as well as to recover the gas distribution described by a five-dimensional map  $f(r, \theta, n_H, N_H, v)$ , where  $\tau$  is the time delay,  $v$  is the observed radial velocity,  $r$  is the distance from the continuum source, and  $\theta$  is the angle from the line of sight. The sensitivity of the emissivities (EW contours in Figure 1) of the optical recombination lines to the continuum flux, and the resulting consequences to their responsivities, make these lines important candidates for inclusion in the quasar tomography. Horne et al. found that when applied to the mostly collisionally excited UV emission lines, a certain amount of ambiguity arises in the recovery of the maps due to the weak dependencies in their EWs (and so responsivities) along lines of constant ionization parameter ( $\propto \Phi_H/n_H$ ) corresponding to their maximum emissivities. Their emissivities and responsivities are largely dependent on  $U_H$ , with smaller dependencies in gas density due to de-excitation or thermalization. The optical recombination lines, along with Mg II  $\lambda 2800$ , offer additional constraints in determining the physical conditions within the BLR, in that their emissivities and responsivities are dependent on the local continuum flux and so radius for a fixed central

continuum luminosity, as well as changes in this flux as the central continuum source varies.

## 5. SUMMARY

The response of the optical recombination lines to continuum variations, especially the Balmer lines, depends critically on the time-averaged photon flux incident on a spatially extended BLR. This strong dependence exists because of the enhanced excited state populations (and so optical depths) that occur at higher continuum flux levels, given the high gas densities found in the BLRs of AGNs. The emissivities, and hence responsivities,  $\eta$ , of these lines are generally strongly anticorrelated with the continuum flux, so  $\eta$  changes with distance within the BLR for a fixed continuum luminosity and with time as the continuum source varies. Below are the major implications, most of which provide explanations for observed relationships:

1. We predict an intrinsic Baldwin effect due to this non-linear response, specifically  $\eta < 1$ , in most emission lines, including the Balmer lines, even after accounting for geometric dilution due to reverberation. This is a finding that has only recently been observationally confirmed. Regarding the optical recombination lines, this effect should be small for He II  $\lambda 4686$  (with responsivity  $\eta \approx 1$ ), but significant for the Balmer lines.
2. We predict that the higher order Balmer lines are more responsive,  $\eta(H\gamma) > \eta(H\beta) > \eta(H\alpha)$ , as is generally observed, and so the broad-line Balmer decrement will steepen in low continuum states, and flatten in high states. Moreover, He II  $\lambda 4686$  should be substantially more responsive ( $0.9 \lesssim \eta \lesssim 1$ ) than the Balmer lines, and so large variations in the broad He II/H $\beta$  integrated flux ratio that are correlated with the continuum state can be expected, even in the absence of a varying continuum SED.
3. A Seyfert 1 galaxy's sub-classification as Seyfert 1.0, 1.5, 1.8, or 1.9 may at least in part be due to the relative flux of ionizing photons present within their broad-line regions at the time of observation. Likewise, any given spectrum of a Seyfert Type 1

AGN may pass through some of these sub-classifications as its continuum luminosity fluctuates from high (Seyfert 1 or 1.5) to low continuum states (Seyfert 1.8 or 1.9).

4. The emission-line responsivity,  $\eta$ , places an additional important constraint on the run of physical conditions within the BLR (e.g., gas density, column density, covering fraction) as a function of radius over and above that of the line emissivity and lag. This is because for the optical recombination lines, the mean responsivity declines with increasing incident photon flux. Thus, for a particular continuum luminosity state, a smaller emissivity-weighted radius is accompanied by a lower effective responsivity.
5. Greater responsivity in the optical recombination lines is expected during low continuum states, and lower responsivity is expected during high continuum states. The characteristic size of the BLR as measured by the emission-line lag also will track the continuum luminosity level, a phenomenon known as "breathing." Responsivities that are functions of the continuum level and hence time result in non-stationary line transfer functions. In this case the time dependence is due to changes in the time-averaged photon flux incident on a spatially extended BLR. The stronger response due to an elevated responsivity at low continuum levels will be enhanced by the greater coherence of an effectively smaller BLR due to breathing. This time-dependence in the line transfer functions should also manifest itself in changes in the line profile widths, with the broad-line component becoming narrower/peakier in high continuum states.
6. Because the emissivities and responsivities of the optical recombination lines are anticorrelated with the incident continuum flux, observations that H $\alpha$ /H $\beta$  and He I/H $\beta$  flux ratios and the Balmer line responsivity decrease from the core to the wings indicate that the BLR velocity field diminishes with increasing distance from the central continuum source. These findings are consistent with recent reverberation studies that find a strong correlation between the emission-line

lag and rms profile width for multiple lines in individual AGNs, which implies that the gas kinematics are dominated by the central massive object.

7. Larger variations in the Balmer decrement with continuum state will be found in the broad-line cores rather than in the wings. Observations of such would also indicate that the BLR velocity field diminishes with increasing distance from the central continuum source.
8. Differences in broad-line widths (whether rms or mean profile) and lags among the Balmer and helium recombination emission lines are in large part due to a radial (continuum flux-dependent) stratification of optical depth effects in these lines.
9. Much of the observed behavior of the optical recombination lines (e.g., the weak response of the Balmer line wings) previously attributed to a substantial contribution from matter-bounded clouds at small BLR radii (i.e., the so-called VBLR) may be explained by the photon flux dependencies of these lines' emissivities and responsivities within ionization-bounded clouds.

These findings should be general, largely independent of any specifically adopted model of the BLR. However, the details of the optical recombination lines' responsivities will be sensitive to and so diagnostic of specific physical conditions within the BLRs of AGNs. In addition to the recombination lines investigated here, we suggest that studies of the IR Paschen and Bracket lines should prove fruitful in further constraining the BLR, particularly in its outer regions.

This paper benefited from the careful and critical review of an anonymous referee. We are grateful to Gary Ferland for maintaining his freely distributed code, Cloudy. We thank the University of St. Andrews and Keith Horne for their hospitality and support through a PPARC visitors grant. We also thank Keith for discussions of work in progress. M.R.G. would like to thank the hospitality and support of Western Michigan University during the completion of this work.



## Appendix: SENSITIVITY OF EMISSION LINE RESPONSIVITY TO MODEL ASSUMPTIONS

We briefly discuss the point that most of the major trends in line responsivity reported here should not depend critically on the particular choice of model for the broad emission-line region. As discussed in § 2, most of these effects can be understood from Figure 1, which shows quite generally the dependence of an emission line’s emissivity on cloud density and incident ionizing photon flux, irrespective of how these clouds (or emitting entities) are distributed or other details.

### A. Cloud Column Densities

Korista et al. (1997) discusses and illustrates the effects of cloud column density on the line emissivities, and thus EW contours in Figure 1. The present simulations assume a constant cloud column density of  $10^{23} \text{ cm}^{-2}$ . In general, the computed integrated AGN line spectrum is relatively insensitive to this parameter for column densities exceeding  $10^{22} \text{ cm}^{-2}$  (see also Goad & Koratkar 1998), except for the high ionization lines of O VI  $\lambda 1034$  and Ne VIII  $\lambda 774$ , which require column densities  $\gtrsim 10^{22.5} \text{ cm}^{-2}$  and  $\gtrsim 10^{23} \text{ cm}^{-2}$  to fully form within the cloud (Korista et al. 1997; Hamann et al. 1998). To the extent that cloud column density has a significant effect on the luminosities or responsivities of the emission lines plotted in Figure 1, the clouds must lie in the vicinity of the central diagonal boundary representing the steep downward gradient in EW (i.e., near  $\log \Phi_H - \log n_H \sim 10.25$ ). These would be the clouds affected by the passage of an ionization front. If the preponderance of clouds have a smaller column density than those computed here, this *diagonal* boundary would shift toward the lower right corners of the density-flux planes in Figure 1. For higher column density clouds, this boundary would shift toward the upper left. The emissivities of clouds lying far from this boundary in the density-flux plane would be essentially unaffected. This is clearly illustrated in Figure 3 of Korista et al. (1997). From Figure 4 and Eq. 2 in the present paper, it can therefore be seen that changing the cloud column density by an order of magnitude in either direction from the adopted value will not change the overall trends of the EW and responsivity of the ionization-bounded clouds being proportional to the incident continuum flux for the four emission lines studied here. Because of their inefficient natures, matter-bounded clouds cannot contribute substantially to the hydrogen recombination line luminosity (or responsivity), unless they have much larger covering fractions than the optically thick clouds at the same radius. Even then, their importance is likely to be minor, except perhaps in the extreme wings given a velocity field that declines with distance from the central source.

### B. Incident Continuum SED, Gas Abundances

Different assumptions about the incident continuum SED or gas abundances do not change the line EW distributions in Figure 1 very much (see Korista et al. 1997), and so would have little effect on these lines’ responsivities.

### C. Optical Depth and Radiative Transfer Effects

If the optical depths in the Balmer lines were significantly reduced by the presence of large extra-thermal velocities that might occur in an accretion disk wind (e.g., Murray & Chiang 1997), the result would be the EW contours in Figure 1 peaking up at higher incident fluxes and densities and the Balmer line-emitting region being more strongly influenced by gas with high responsivity ( $\eta \approx 1 - 2$ ). Since the Balmer lines have reported responsivities less than 1 even after correcting for geometric dilution, this would constrain models with large extra-thermal velocities and/or Balmer emission from large outer radii. Other consequences of significant extra-thermal velocities might be smaller predicted lags and broader predicted line profiles (for a fixed central mass and incident continuum luminosity). If in general the radiative transfer of the Balmer lines is currently less than adequately handled (as may be the case; see Netzer et al. 1995), the optical depth of  $H\alpha$  should nevertheless remain greater than that of  $H\beta$ , and those of the helium lines should remain smaller

than the Balmer lines. Thus, the relative senses of the EW contours of the Balmer lines in Figure 1 should be preserved. The sense of the Balmer decrement variability as a function of continuum state should also be preserved, as should the  $H\alpha/H\beta$  intensity ratio across the line profile: *provided that the bulk of the velocity field diminishes with increasing distance from the central source.*

#### **D. Possible Alternate Trends in Lag and Line Response**

Most of the extra responsivity in  $H\beta$  over  $H\alpha$  in Figure 7 lies within the line core whose contributions are dominated by gas lying (and responding) at larger distances. As a consequence, the difference in the measured lags of these two lines may not be as large as their EW distributions in Figure 1 might indicate. That is, their responsivity-weighted radii may be closer in size than their emissivity-weighted radii (Goad et al. 1993). In fact, depending on the actual emissivity and responsivity distributions of the two lines, it is possible for  $H\beta$  to lag slightly behind  $H\alpha$ . In other words the total light profile may be broader in  $H\beta$  than  $H\alpha$  and the other way around in the rms variation profile, with  $H\alpha$  having a slightly smaller lag. The small differences in the Balmer lines' beaming functions (O'Brien et al. 1994) may also play a role in altering the relative responsivity-weighted radii, and thus relative lags of these emission lines.

## REFERENCES

- Antonucci, R.J., & Cohen, R.D. 1983, ApJ, 271, 564
- Baldwin, J.A., Korista, K.T., Ferland, G.J., & Verner, D.A. 1995, ApJ, 455, L119
- Boroson, T.A., & Green, R.F. 1992, ApJS, 80, 109
- Bottorff, M.C., Korista, K.T., Shlosman, I., & Blandford, R.D. 1997, ApJ, 479, 200
- Bottorff, M.C., Baldwin, J.A., Ferland, G.J., Ferguson, J.W., & Korista, K.T. 2002, ApJ, 581, 932
- Carroll, T.J. 1985, MNRAS, 214, 321
- Carroll, T.J., & Kwan, J. 1985, ApJ, 288, 73
- Clavel, J., et al. 1991, ApJ, 366, 64
- Corbin, M. 1995, ApJ, 447, 496
- Corbin, M. 1997, ApJS, 113, 245
- Corbin, M., & Smith, P. 2000, ApJ, 532, 136
- Crenshaw, D.M. 1986, ApJS, 62, 821
- Davidson, K., & Netzer, H. 1979, Rev. Mod. Phys., 51, 715
- Dietrich, M., et al. 1993, ApJ, 408, 416
- Ferguson, J.W., Korista, K.T., Baldwin, J.A., & Ferland, G.J. 1997, ApJ, 487, 122
- Ferland, G.J., 1997, HAZY, A Brief Introduction to Cloudy (Univ. Kentucky Phys. Dept. Int. Rep.)
- Ferland, G.J., Korista, K.T. & Peterson, B.M. 1990, ApJ, 363, L21
- Ferland, G.J., Korista, K.T., Verner, D.A., Ferguson, J.W., Kingdon, J.B., & Verner, E.M. 1998, PASP, 110, 761
- Ferland, G.J., & Netzer, H. 1979, ApJ, 229, 274
- Ferland, G.J., & Netzer, H., & Shields, G. 1979, ApJ, 232, 382
- Ferland, G.J., Peterson, B.M., Horne, K.D., Welsh, W.F., & Nahar, S.N. 1992, ApJ, 387, 95
- Fromerth, M.J., & Melia, F. 2000, ApJ, 533, 172
- Gilbert, K., & Peterson, B.M. 2003, ApJ, 587, 123
- Goad, M.R., & Koratkar, A.P. 1998, ApJ, 495, 718
- Goad, M.R., O'Brien, P.T., & Gondhalekar, P.M. 1993, MNRAS, 263, 149
- Goad, M.R., Koratkar, A.P., Axon, D.J., Korista, K.T., & O'Brien, P.T. 1999, ApJ, 512, L95
- Gondhalekar, P.M. 1987, in "Emission Lines in Active Galactic Nuclei," Proceedings of a Workshop on Astronomy and Astrophysics (Chilton, England: Rutherford Appleton Laboratory), ed. P.M. Gondhalekar
- Gondhalekar, P.M. 1990, MNRAS 243, 443.
- Hamann, F., Cohen, R.D., Shields, J.C., Burbidge, E.M., Junkkarinen, V., & Crenshaw, D.M. 1998, ApJ, 496, 761
- Horne, K., Korista, K.T., & Goad, M.R. 2003, MNRAS, 339, 367
- Kaspi, S., & Netzer H. 1999, ApJ, 524, 71
- Kassebaum, T.M., Peterson, B.M., Wanders, I., Pogge, R.W., Bertram, R., & Wagner, R.M. 1997, ApJ, 475, 106
- Kinney, A.L., Rivolo, A.R., & Koratkar, A.R. 1990, ApJ, 357, 338
- Kollatschny, W. 2003, A&A, 407, 461

Korista, K.T., et al. 1995, ApJS, 97, 285 (K95)

Korista, K., Baldwin, J., Ferland, G., Verner, D. 1997, ApJS, 108, 401

Korista, K.T., & Goad, M.R. 2000, ApJ, 536, 284 (KG00)

Korista, K.T., & Goad, M.R. 2001, ApJ, 553, 695

Krolik, J.H., Horne, K., Kallman, T.R., Malkan, M.A., Edeleson, R.A., & Kriss, G.A. 1991, ApJ, 371, 541

Kwan, J. 1984, ApJ, 283, 70

Maoz, D., et al. 1993, ApJ, 404, 576

Marshall, H., et al. 1997, ApJ, 479, 222

Marziani, P., & Sulentic, J.W. 1993, ApJ, 409, 612

Murray, N., & Chiang, J. 1997, ApJ, 474, 91

Morris, S.L., & Ward, M.J. 1989, ApJ, 340, 713

Netzer, H. 1975, MNRAS, 171, 395

Netzer, H. 1978, ApJ, 219, 822

Netzer, H. in Active Galactic Nuclei, (Springer-Verlag: 1991), p.57

Netzer, H., et al. 1990, ApJ, 353, 108

Netzer, H., Brotherton, M.S., Wills, B.J., Han, M., Wills, D., Baldwin, J.A., Ferland, G.J., & Browne, I.W.A. 1995, ApJ, 448, 27

Netzer, H., & Maoz, D. 1990, ApJ, 365, L5

O'Brien, P.T., Goad, M.R., & Gondhalekar, P.M. 1994, MNRAS, 268, 845

O'Brien, P.T., Goad, M.R., & Gondhalekar, P.M. 1995, MNRAS, 275, 1125

O'Brien, P.T., Zheng, W., & Wilson, R. 1989, MNRAS, 240, 741

Onken, C.A., & Peterson, B.M. 2002, ApJ, 572, 746

Osterbrock, D.E., in Astrophysics of Gaseous Nebulae and Active Galactic Nuclei, (University Science Books: 1989), pp.312-313

Osterbrock, D.E. & Shuder, J.M. 1982, ApJS, 49, 149

Paltani, S., & Courvoisier, T.J.-L. 1994, A&A, 291, 74

Paltani, S., & Walter, R. 1996, A&A, 312, 55

Pérez, E., Penston, M.V., & Moles, M. 1989, MNRAS, 239, 55

Pérez, E., Robinson, A., & de la Fuente, L. 1992, MNRAS, 255, 502

Perry, J.J., van Groningen, E., & Wanders, I. 1994, MNRAS, 271, 561

Peterson, B.M. 1997, An Introduction to Active Galactic Nuclei (Cambridge University Press)

Peterson, B.M., & Ferland, G.J. 1986, Nature, 324, 345

Peterson, B.M., et al. 1991, ApJ, 368, 119

Peterson, B.M., Ali, B., Horne, K., Bertram, R., Lame, N.J., Pogge, R.W., & Wagner, R.M. 1993, ApJ, 402, 469

Peterson, B.M., et al. 1999, ApJ, 510, 659

Peterson, B.M., et al. 2000, ApJ, 542, 161

Peterson, B.M., et al. 2002, ApJ, 581, 197

Peterson, B.M., & Wandel, A. 1999, ApJ, 521, L95

Peterson, B.M., & Wandel, A. 2000, ApJ, 540, L13  
Pogge, R.W., & Peterson, B.M. 1992, AJ, 103, 1084  
Rees, M.J., Netzer, H., & Ferland, G.J. 1989, ApJ, 347, 640  
Robinson, A., Pérez, E., & Binette, L. 1990, MNRAS, 246, 349  
Romanishin, W. et al. 1995, ApJ, 455, 516  
Shields, J.C., & Ferland, G.J. 1993, ApJ, 402, 425  
Shields, J.C., Ferland, G.J., & Peterson, B.M. 1995, ApJ, 441, 507  
Shuder, J.M. 1982, ApJ, 259, 48  
Shuder, J.M. 1984, ApJ, 280, 491  
Sparke, L.S. 1993, ApJ, 404, 570  
Stirpe, G.M. 1990, A&AS, 85, 1049  
Stirpe, G.M. 1991, A&A, 247, 3  
Stirpe, G.M. de Bruyn, A.G., & van Groningen, E. 1988, A&A, 200, 9  
Sulentic, J., Marziani, P., Zwitter, T., Dultzin-Hacyan, D., & Calvani, M. 2000, ApJ, 545, L15  
Tran, H.D., Osterbrock, D.E., & Martel, A. 1992, AJ, 104, 2072  
Vanden Berk, D.E., et al. 2004, ApJ, 601, 692  
van Groningen, E. 1984, Thesis, Sterrewacht Leiden  
van Groningen, E. 1987, A&A, 186, 103  
Wamsteker, W., et al. 1990, ApJ, 354, 446  
Wanders, I. 1994, in ASP Conf. Ser. 69, Reverberation Mapping of the Broad-Line Region in Active Galactic Nuclei, ed. P.M. Gondhalekar, K. Horne, & B.M. Peterson (San Francisco: ASP), 127  
Wanders, I., & Peterson, B.M. 1996, ApJ, 466, 174  
Zheng, W. 1992, ApJ, 385, 127

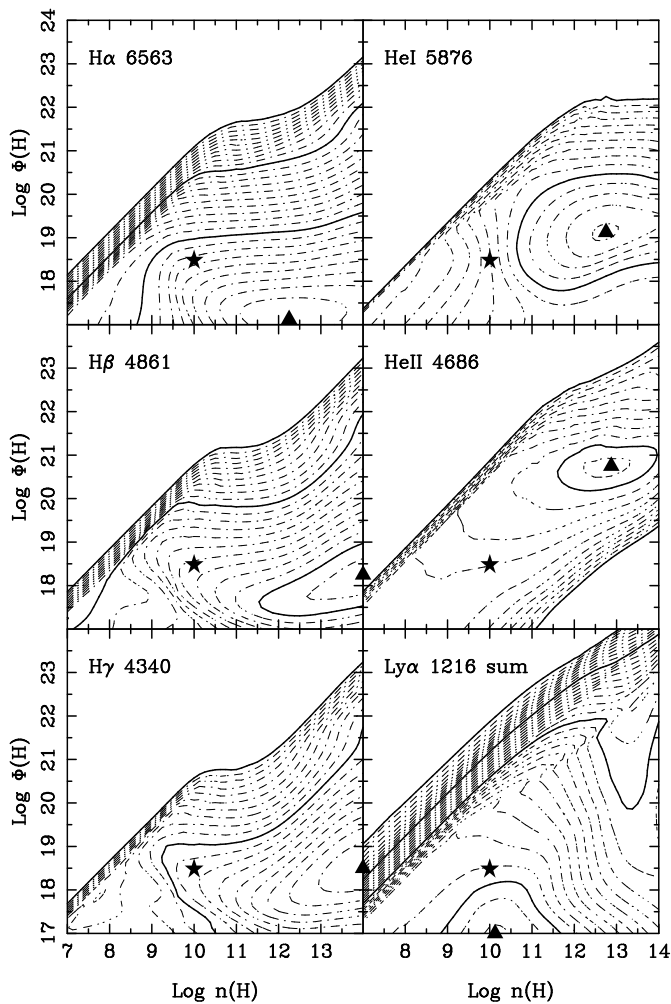


Fig. 1.— Contours of  $\log W_\lambda$  (EW) for six emission lines, *referenced to the incident continuum at 1215 Å*, are shown as a function of the hydrogen number density and flux of hydrogen-ionizing photons for full source coverage at every position. The total hydrogen column density is  $10^{23} \text{ cm}^{-2}$ . The EW is in direct proportion to the continuum reprocessing efficiency. The smallest decade contour (generally running diagonally through the centers of the diagrams) corresponds to 1 Å, each solid line is 1 decade, and dash-dotted lines represent 0.1 decade steps. The contours decrease monotonically from the peak (*triangle*) to the 1 Å contour, and the blank regions in the upper left portion of the panels have EWs less than 1 Å. The star in each panel is a reference point marking the old “standard BLR” parameters (Davidson & Netzer 1979).

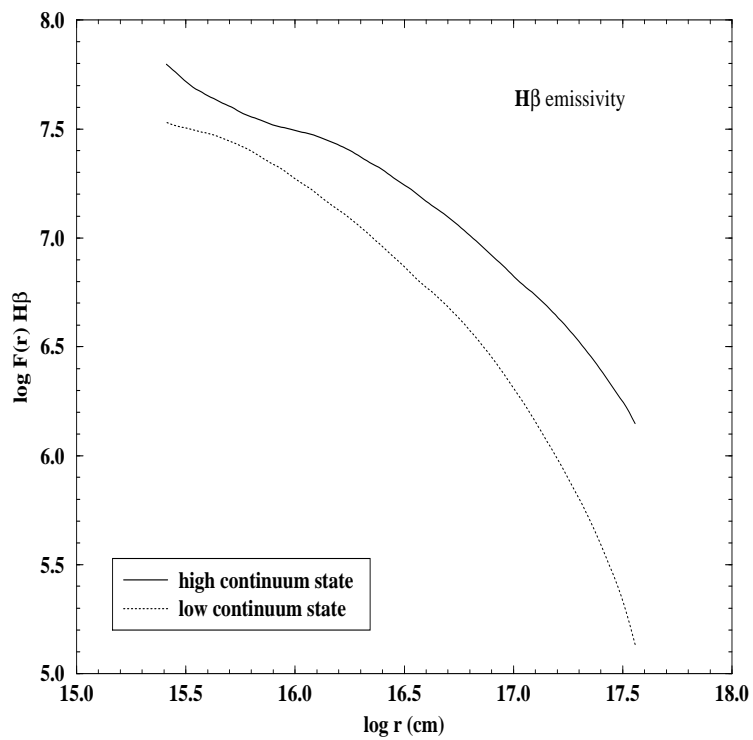


Fig. 2.— Effective logarithmic  $H\beta$  surface flux ( $\text{ergs s}^{-1}\text{cm}^{-2}$ ) versus the logarithm of the distance from the ionizing continuum source for the two continuum states. The  $H\beta$  emissivities of clouds with a range of gas densities have been summed at each radius.

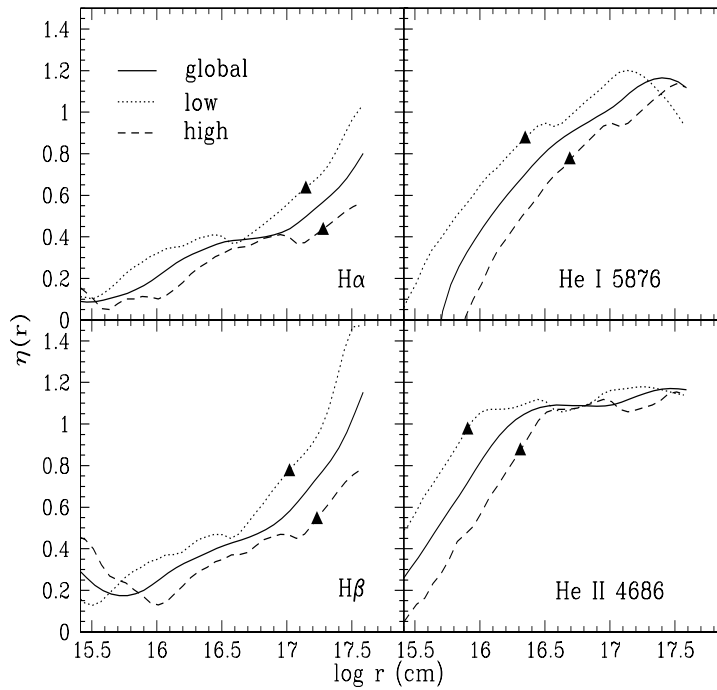


Fig. 3.— Radial responsivities of the four recombination lines under study. The solid line represents the responsivity for the factor of 8.2 change in continuum flux. The dotted line represents the same for 10% variations about the low continuum state, and the dashed line for 10% variations about the high continuum state. The responsivity-weighted radius is marked with a triangle for each of the latter two cases.



Fig. 4.— Same as Fig. 1, but with a superposed gray scale in responsivity. White represents  $\eta < 0$ . The lightest shade of gray represents  $0 \leq \eta < 0.5$ , medium gray  $0.5 \leq \eta < 1.0$ , medium dark gray  $1.0 \leq \eta < 1.5$ , dark gray  $1.5 \leq \eta < 2.0$  (appearing in He II  $\lambda 4686$ , H $\beta$ , H $\gamma$  only), and black  $\eta \geq 2$  (appearing only in the panel for He II  $\lambda 4686$ , which shows all of the shades). These responsivities were computed for 0.45 decades (factor of 2.8) variations in the continuum luminosity about the adopted mean continuum state.

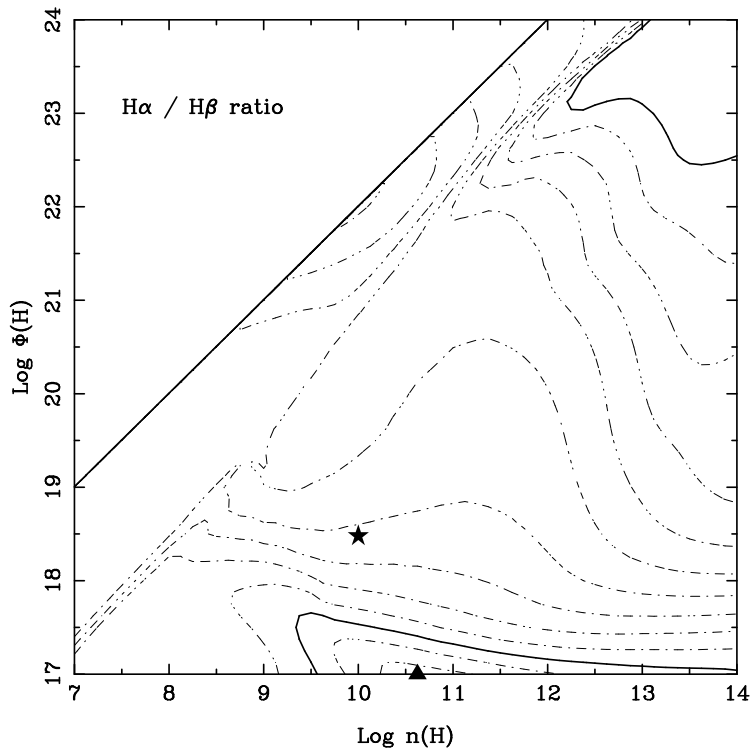


Fig. 5.— Logarithmic flux ratios of  $\text{H}\alpha/\text{H}\beta$  in the density-flux plane. The solid contour near the bottom of the diagram represents a flux ratio of 10 (1.0 in the log), the dash-dotted contours are 0.1 decade intervals, and the solid contour in the upper right corner represents a flux ratio of 1.0 (0.0 in the log). The triangle lies at the peak ratio of  $\approx 17$ . The star is a reference point marking the old “standard BLR” parameters of Davidson & Netzer (1979), and has a value of  $\approx 4.2$ . The contours end abruptly at the central diagonal solid line, where the equivalent widths of the two lines become very small due to the extremely high ionization state of the gas.

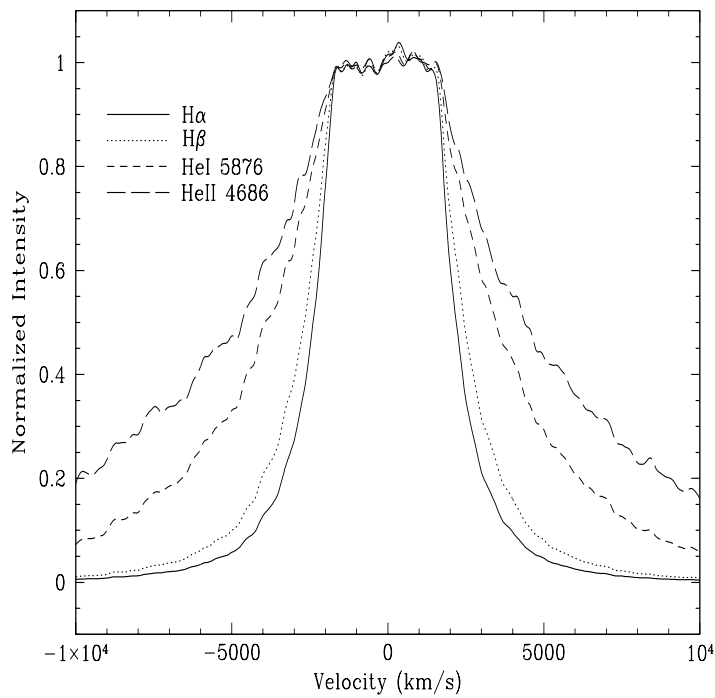


Fig. 6.— Model emission-line profiles for the four recombination lines under study, scaled to their peak intensities to ease comparison. See § 3.5 for details.

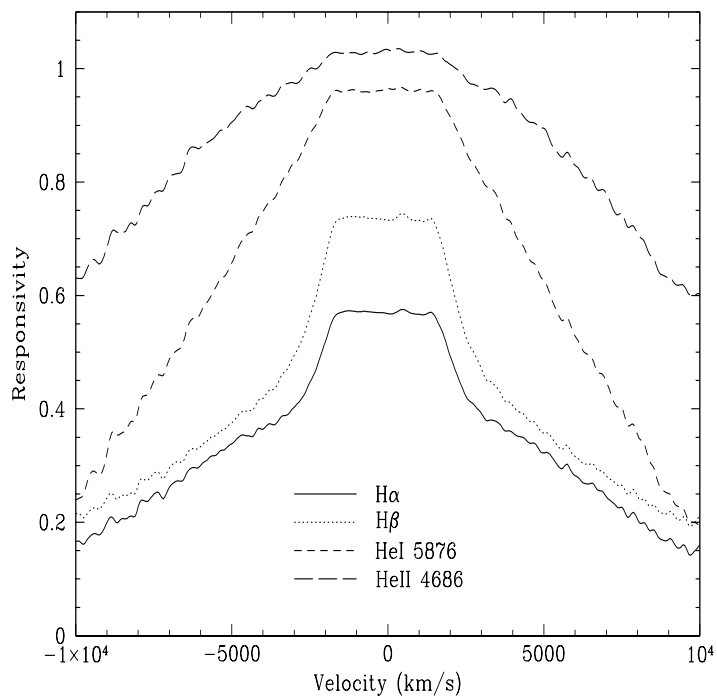


Fig. 7.— Model emission-line responsivities presented as functions of radial velocity for the four recombination lines under study (§ 3.5).

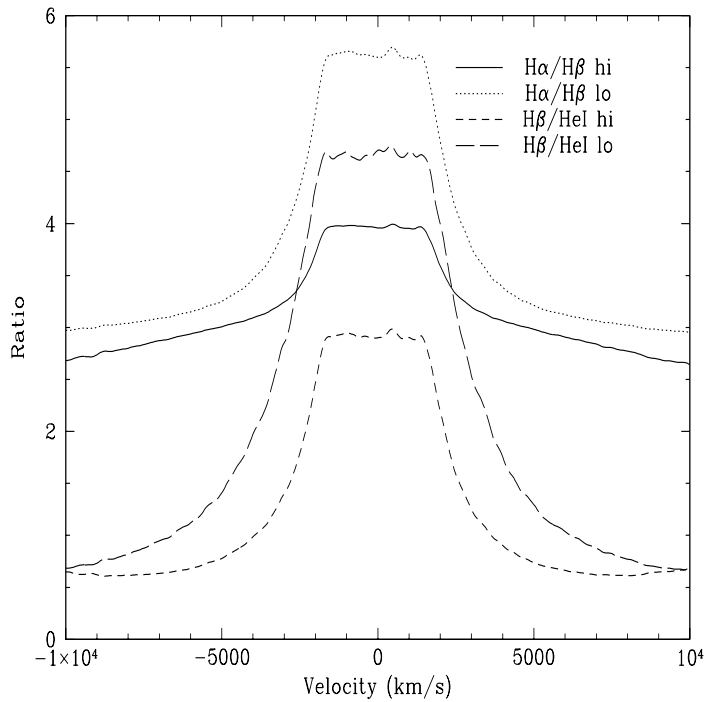


Fig. 8.—  $H\alpha/H\beta$  and  $H\beta/He\ I\ \lambda 5876$  flux ratios presented as functions of radial velocity in the low and high continuum states (§ 3.6). In both cases, the smaller ratios are found in the high continuum states because of the stronger response of the line in the ratio's denominator.

Table 1: Model Effective Line Responsivity & Profile Variability

Emission Line	$\eta_{eff}(\text{global})$	$\eta_{eff}(\text{hi})$	$\eta_{eff}(\text{lo})$	FWHM(hi) (km/s)	FWHM(lo) (km/s)
H $\alpha$ $\lambda$ 6563	0.52	0.43	0.63	4200	4600
H $\beta$ $\lambda$ 4861	0.64	0.54	0.77	4510	5230
H $\gamma$ $\lambda$ 4340	0.68	0.58	0.79	4570	5250
He I $\lambda$ 5876	0.83	0.77	0.87	5780	7350
He II $\lambda$ 4686	0.92	0.87	0.97	7590	9480
Ly $\alpha$ $\lambda$ 1216	0.74	0.71	0.77	5180	5280

This figure "f4.jpeg" is available in "jpeg" format from:

<http://arxiv.org/ps/astro-ph/0402506v2>